ADVANCED ELECTRONIC MATERIALS Open Access
www.advelectronicmat.de

Spatiotemporal Microscopy: Shining Light on Transport Phenomena

Guillermo D. Brinatti Vazquez, Giulia Lo Gerfo Morganti, Alexander Block, Niek F. van Hulst, Matz Liebel, and Klaas-Jan Tielrooij**

Transport phenomena like diffusion, convection, and drift play key roles in the sciences and engineering disciplines. They belong to the most omnipresent and important phenomena in nature that describe the motion of entities such as mass, charge or heat. Understanding and controlling these transport phenomena is crucial for a host of industrial technologies and applications, from cooling nuclear reactors to nanoscale heat-management in the semiconductor industry. For decades, macroscopic transport techniques have been used to access important parameters such as charge mobilities or thermal conductivities. While being powerful, they often require physical contacts, which can lead to unwanted effects. Over the past years, an exciting solution has emerged: a technique called spatiotemporal microscopy (SPTM) that accesses crucial transport phenomena in a contactless, all-optical, fashion. This technique offers powerful advantages in terms of accessible timescales, down to femtoseconds, and length scales, down to nanometres, and, further, selectively observes different species of interest. This tutorial review discusses common experimental configurations of SPTM and explains how they can be implemented by those entering the field. This review highlights the broad applicability of SPTM by presenting several exciting examples of transport phenomena that were unravelled thanks to this technique.

1. Introduction

1.1. Motivation

The transport phenomenon of diffusion describes the motion of a species due to a concentration gradient. Microscopically, this involves a random walk – the so-called Brownian motion – and is described by simple physical laws: Fick's law for particle diffusion and Fourier's law for heat diffusion. These are mathematically identical and contain just one parameter that describes the efficiency of motion, which is called the diffusivity, D. The transport phenomenon of convection, called drift in the case of charge transport, describes motion as a result of other forces, for example created by the presence of an electric field. By studying transport phenomena, one can learn a great deal about the microscopic processes that take place in a material or system, such as momentum scattering mechanisms that govern charge and heat transport, including electron–phonon, electron-impurity, electron–electron, and phonon–phonon interactions, and the role of charge traps. This understanding is crucial for (opto)electronic and thermal applications.

Some conventional techniques aimed at understanding charge transport are field-effect measurements and Hall measurements, which involve the application of an electrical and/or magnetic field, combined with the measurement of the generated current or voltage. Heat transport measurements often use electrical heaters to create a thermal temperature difference, which allows measuring heat flow with a simple thermometer. These are powerful and broadly applied techniques that

G. D. B. Vazquez, G. L. G. Morganti, N. F. van Hulst
ICFO-Institut de Ciencies Fotoniques
The Barcelona Institute of Science and Technology
Castelldefels, Barcelona 08860, Spain

The ORCID identification number(s) for the author(s) of this article can be found under https://doi.org/10.1002/aelm.202300584

DOI: 10.1002/aelm.202300584

A. Block, K.-J. Tielrooij
Catalan Institute of Nanoscience and Nanotechnology - ICN2 (BIST and CSIC)
Campus UAB, Bellaterra, Barcelona 08193, Spain
E-mail: klaas.tielrooij@icn2.cat

N. F. van Hulst
ICREA-Institució Catalana de Recerca i Estudis Avançats
Passeig Lluís Companys 23, Barcelona 08010, Spain

M. Liebel
Department of Physics and Astronomy
Vrije Universiteit Amsterdam
De Boelelaan 1081, Amsterdam 1081 HV, The Netherlands
E-mail: m.liebel@vu.nl

K.-J. Tielrooij
Department of Applied Physics
TU Eindhoven
Den Dolech 2, Eindhoven 5612 AZ, The Netherlands

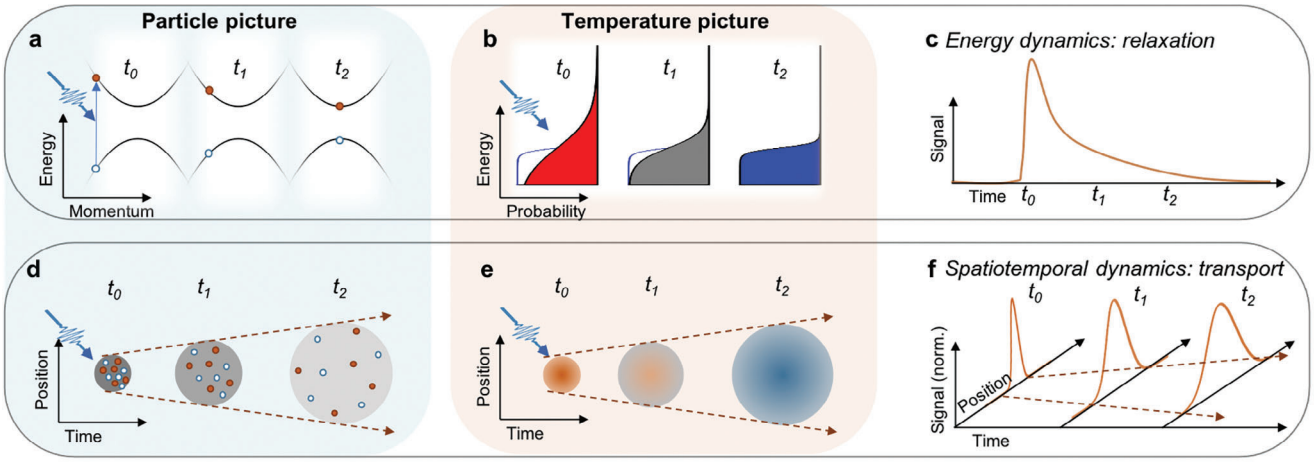

Figure 1. Temporal versus spatiotemporal heat and particle dynamics. a) Example of an energy relaxation process of a particle. At time-zero, t_0, photoexcitation creates an electron-hole pair with excess kinetic energy, which is lost over time via energy relaxation. b) Example of an energy relaxation process of electronic heat. At time-zero, t_0, photoexcitation creates an electron distribution with an elevated temperature. The initially broadened, hot, distribution cools over time. c) Example of a time-resolved measurement, where the temporal signal decrease corresponds to energy relaxation (cooling dynamics) of photoexcited particles (heat). d) Schematic of the spatiotemporal dynamics of photoexcited particles. As time progresses, the initially localized particles radially diffuse in space. e) Schematic of the spatiotemporal dynamics of photo-induced heat, where the photoexcited, localized, "hot spot" radially diffuses in space. f) Example of a spatiotemporal measurement, where the normalized position-dependent signal spatially broadens in time, thus directly revealing transport phenomena.

provide the electrical or thermal conductivity of a system. They indirectly report on the microscopic interactions that govern charge and heat transport. However, these "macroscopic" transport techniques do require the fabrication of electrical and/or thermal contacts to a material or system under study. Furthermore, they sometimes suffer from unwanted effects, such as contact resistance and undesired heat sinks. Moreover, they do not always allow distinguishing different species – electrons or holes, singlet or triplet excitons, etc. And finally, they report temporally and spatially averaged properties. In particular, it is challenging to directly access the microscopic interactions that take place on sub-nanosecond timescales and sub-micron length scales.

Over the years, methods have been developed that overcome some of these limitations. Optical techniques are especially powerful in that regard as they do not require electronic contacts and specifically access species of interest via wavelength selectivity. A particularly promising emerging optical transport technique is spatiotemporal microscopy (SPTM) which, as the name suggests, provides combined spatial and temporal resolution. It enables the non-contact study of transport phenomena in a very intuitive fashion by visualizing the spatial spreading of a certain species as a function of time. As such, it directly accesses the species' transport dynamics.

1.2. This Review

In this review, we will describe the main experimental implementations of SPTM and discuss how they can be used to study particle and heat transport. To underscore the broad applicability of SPTM we will highlight several interesting physical phenomena that have been discovered thanks to this measurement technique. We will show that SPTM is an extremely useful and versatile technique that not only complements more traditional transport techniques, but also provides access to information that is otherwise difficult or impossible to obtain. This review provides the necessary guidelines for scientists and engineers interested in integrating SPTM into their characterization workflow, or for those who aim to study physical phenomena at previously inaccessible temporal and spatial regimes. We note that this is not an exhaustive overview of all existing spatiotemporal techniques and measurements. Finally, we refer the interested reader to two existing reviews that cover some aspects of SPTM.[1,2]

In the context of this review, we will consider transport governed by two different groups of species: i) particles or quasi-particles, such as electrons, holes, excitons, plasmons, etc. (**Figure** 1a) and ii) heat, typically electronic heat or phononic heat (Figure 1b). Section 2 discusses different observable signals and describes the main experimental implementations of SPTM. In Section 3, we briefly summarize some theoretical aspects of transport physics, in particular drift-diffusion. Section 4 discusses recent physical discoveries related to particle transport based on spatiotemporal studies and Section 5 highlights those related to heat transport. Finally, Section 6 concludes this review with an outlook on where we believe the field is heading.

2. The Technique of SPTM

2.1. General Concept

Time-resolved optical measurements enable the study of dynamic sample responses, typically by examining signals at precisely controlled temporal delays after photoexcitation. Such approaches provide valuable insights into fundamental physical and chemical processes that are usually related to energy

dynamics or relaxation. Microscopically, a "particle picture" is often used for describing relaxation processes governed by interactions, such as exciton–exciton annihilation, electron–phonon coupling, charge separation or energy transfer. In this case, one considers the dynamics of certain particles or quasi-particles – electrons, phonons, excitons, plasmons, magnons, etc. (Figure 1a). There are also phenomena where a statistical mechanics, "thermodynamic picture" is more suitable. In this case, one considers the dynamics of the temperature and chemical potential of a (sub)system, such as the electron or phonon ensembles (Figure 1b).

The basic principle behind time-resolved optical measurements is to first illuminate a sample with a short optical pulse, and then to detect the photoinduced response at a precisely defined time-delay afterwards. This allows the study of dynamical processes with a temporal resolution down to the femtosecond (10^{-15} s) regime, although even the attosecond regime (10^{-18} s) is attainable in certain setups. A typical measurement yields a time-dependent signal, where photoexcitation occurs at time-zero (t_0). The result is a rapid signal change at time-zero, followed by signal decay, which reports on the system's evolution and underlying relaxation phenomena (Figure 1c).

The crucial innovation of SPTM, as compared to "conventional" time-resolved optical measurements, is the addition of the spatial degree of freedom. In spatiotemporal measurements, photoexcitation is spatially confined to a small area and the out-of-equilibrium, or quasi-equilibrium, system evolves both temporally and spatially. In the "particle picture", absorption of light leads to the photoexcitation of particles, which then spread out in space as time evolves (Figure 1d). If no external fields are applied, this process is driven by a concentration gradient as described by Fick's law: the particle diffusivity describes how fast the particles spread in space (see also Section 3). In the "temperature picture", photoexcitation locally heats the system, after which the localized heat spatially spreads (Figure 1e). In the absence of external fields, Fourier's law describes this thermal gradient-driven process (see also Section 3). The thermal diffusivity, often referred to as the measure of how quickly heat spreads spatially, quantifies the rate at which temperature changes propagate through a material.

A typical spatiotemporal measurement results in a 2D map that contains the signal as a function of space and time. At specific time delays, e.g., t_0, t_1, and t_2, the spatial profiles will look different, typically broadening for increasing time delays, as a result of transport processes, such as diffusion (Figure 1f). The extent to which spatial broadening occurs over time provides information about the particle or thermal diffusivity (see also Section 3): This is the essence of SPTM.

2.2. Experimental Implementations of SPTM

SPTM setups require several key components to simultaneously achieve high temporal and high spatial resolution. Temporal resolution is commonly ensured by the use of pulsed lasers that enable temporal resolutions down to the femtosecond level. Spatial resolution is ensured by spatially encoded photoexcitation, often by confining light to a small area using a high numerical aperture objective. This results in (near-)diffraction-limited spots with typically sub-micrometer widths for visible light. Tracking the transport of this photoexcitation in space and time can be done via different approaches. We will outline four main implementations in more detail below: time-correlated microscopy, widefield imaging, point scanning, and grating-based techniques.

The choice of technique is often based on a trade-off between experimental complexity and aspects related to photodamage or signal-to-noise ratios. The latter is important as it determines how precisely transport-driven spatial broadening can be resolved. This can be well below the excitation spot size, and even below the optical diffraction limit: with a good enough signal-to-noise ratio, it is possible to observe how a micrometer-sized spatial profile broadens by just a few nanometers. Pump-modulation/demodulation schemes are the go-to methodology for ensuring operation near the shot-noise limit, thus providing the best possible signal-to-noise ratios. Typical implementations involve modulation of the pump pulse at a fixed frequency using acousto-optic or electro-optic modulators, or a mechanical chopper. Demodulation at the same frequency then isolates the pump-induced signals and, conveniently, rejects all noise contributions outside a narrow band around the modulation frequency.

SPTM is extremely versatile, as it only requires an optically or optoelectronically-accessible signal – a prerequisite that is met by most samples. Optically, SPTM can be based on spontaneously emitted, linear, as well as nonlinear, transient, signals. Fluorescence and phosphorescence allow accessing the former. Signatures of excited electronic or phononic states can be measured via nonlinear spectroscopy. Electronic excitations can be visualized by probing spectral windows reporting on ground state bleach, excited state absorption or stimulated emission. Phononic excitation, or phonon heat, is accessible via pump-induced refractive index changes, e.g., via the material's thermo-optic coefficient. An emerging, alternative, approach is based on directly detecting optoelectronic signals as, for example, optically-induced photocurrent.

Ultimately, the signals outlined above report on the sample's transport parameters and it is often possible to obtain compatible information via different routes. Experimentally, the ideal strategy is sample- and question-dependent and parameters such as signal levels, damage thresholds, spectral position of electronic transitions or decay timescales often impact the choice. In the following, we introduce the most commonly used experimental implementations of SPTM, in order to guide the reader toward determining suitable approaches for a research question of interest.

2.2.1. Time-Correlated Microscopy

Fast electronics, operating in the pico- to nanosecond regime, directly access emission kinetics in the form of luminescence lifetimes. When combined with confocal detection and pump-position scanning, these approaches enable straightforward SPTM based on linear signals: the fast electronics provide the temporal information, position-scanning the spatial information. **Figure 2**a depicts a typical experimental implementation. The pump pulse generates spatially-defined carriers that spontaneously emit a signal, e.g., luminescence. This signal is

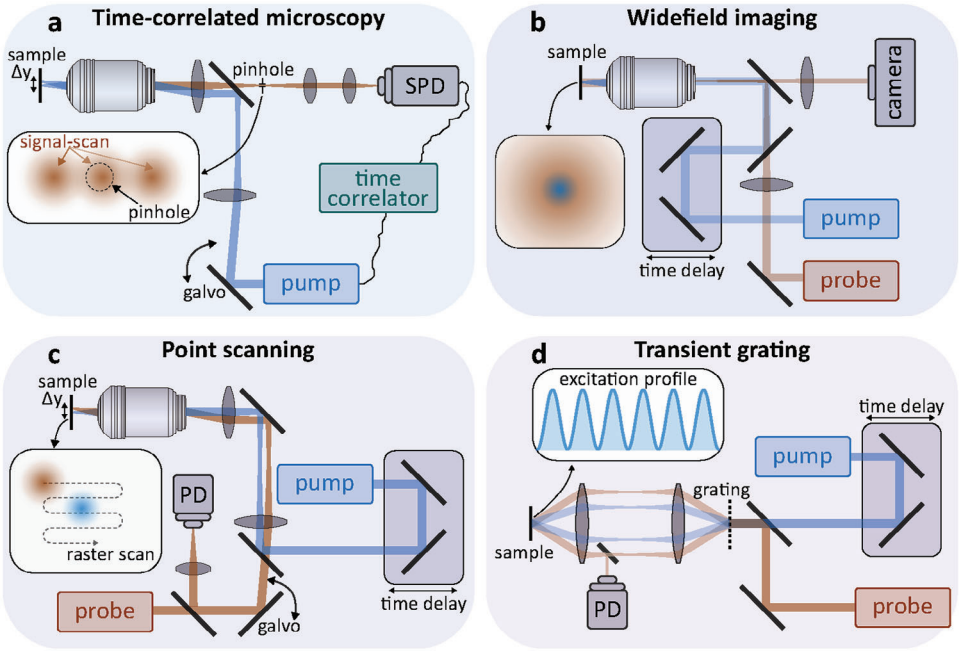

Figure 2. Four flavors of SPTM. a) Time-correlated microscopy where excitation-scanning combined with a fast electronic detector quantifies diffusion dynamics. b) SPTMbased on widefield imaging the spatiotemporal evolution of an, initially, localised signal. c) Point-scanning implementation of SPTM. d) Transient grating experiment that indirectly quantifies diffusion dynamics by imprinting a high-frequency grating-excitation onto the sample. SPD = single photon detector; galvo = galvanometric mirrors; PD = photodetector.

collected by a microscope, imaged onto a pinhole and then propagated onto a fast single photon detector, such as an avalanche photodiode. A time correlator registers the photon arrival times with respect to the time of photoexcitation by the pump pulse, an approach called time-correlated single photon counting. Employing a pinhole that is smaller than the pump-spot spatially selects parts of the emitted signals. As such, it is possible to sample the photoinduced signal as a function of both time and relative distance with respect to the pump. Systematically recording temporal arrival times for many different relative pump-to-pinhole positions yields the desired spatiotemporal information. Experimentally, galvanometric mirrors are used for pump-scanning. Alternatively, a translation stage-mounted pinhole or detector can be employed.

Although time-correlated microscopy is slower than the pump-probe alternatives discussed in the following sections, it offers some unique advantages. First, only one pulse is required, which considerably reduces the experimental complexity. Commercial confocal microscopes with fluorescence lifetime imaging capabilities can be easily adapted for this purpose. Second, the experiments are of linear nature. It is thus possible to operate at lower pump fluences as compared to nonlinear measurements. Lastly, the detected photons often originate from a well-defined electronic state, which can greatly facilitate signal interpretation. Very fast processes, on femtosecond timescales, and non-emissive states are, however, difficult to access.

More detailed information on time-correlated spatiotemporal setups can be found in the literature. Specifically, for the use of a streak camera see Ref. [3], for a scanning APD or pinhole in detection see Ref. [4–7], while for scanning excitation with a fixed APD detector see Refs. [8].

2.2.2. Widefield Pump-Probe Imaging

Figure 2b schematically depicts a typical widefield-imaging based pump-probe experiment. A tightly focused pump excites the sample and a considerably larger, often collimated, probe interrogates it at a precisely defined pump-probe delay. A camera ultimately detects a sample-image, as seen by the probe, in either a reflection or transmission geometry. Subtracting two images, acquired in the presence, "*pump ON*", and absence, "*pump OFF*", of the pump-pulse isolates the pump-induced transient signal. Capturing many of these differential "*pump ON - pump OFF*" images, while systematically varying the pump-probe delay then yields the desired spatiotemporally-resolved information.

In more detail, pump and probe pulses are mostly derived from the same laser source where additional (nonlinear) wavelength-conversion steps, via, for example, second harmonic generation or parametric amplification, allow tuning the pulses to match the spectral resonances of interest. A mechanical delay-line controls the time-delay between the pulses and allows accessing femto- to nanosecond delays. Longer delays, in the nanoseconds to seconds range, are accessible by combining two electronically synchronized lasers. The pump and probe beams are recombined to travel collinearly, pass a beamsplitter, and enter the microscope objective. The pump pulse enters in a collimated fashion and is hence tightly focused in the sample plane. The probe is focused into the back-focal-plane of the microscope objective, and therefore interrogates the sample in a collimated fashion. When operating in a reflection geometry, the same microscope objective collects the signal which then passes the beamsplitter where a lens forms an image of the sample plane on a camera. In transmission, a second objective collects the signal followed by

image formation via an additional lens. In both cases, additional filters, such as bandpass or notch-filters, reject residual pump light prior to image formation to ensure that only pump-induced probe changes are detected and not the, orders-of-magnitude larger, modulation-induced pump-intensity changes.

Widefield-based approaches are experimentally relatively straightforward to implement, especially in their reflection form. Existing pump-probe setups can be readily upgraded to access spatiotemporal information by incorporating a microscope objective and a camera. However, compared to photodiodes, cameras are slow, costly, and exhibit very limited dynamic ranges, even for high-end solutions. Nevertheless, widefield detection is often sufficiently sensitive to study many samples. Additionally, widefield observations provide very intuitive feedback as the sample is visualized in real time. As such, widefield approaches represent an excellent starting point for those interested in SPTM.

For more detailed information on widefield SPTM setups, please see Refs. [9–11].

2.2.3. Point-Scanning, Confocal Detection

Figure 2c shows the basic configuration of a point scanning spatiotemporal microscope, which relies on tightly focused pump and probe pulses. The time delay is controlled with a mechanical delay line, as previously. To recover spatial information a galvanometric *xy*-scanner, placed in a conjugate Fourier plane of the microscope objective's back-focal-plane, spatially scans the probe across the static pump focus. The reflected, or transmitted, probe beam is collected, isolated, e.g., via a dichroic filter, and detected by a point detector, such as a photodiode. The spatiotemporal signal of interest is recovered via images that are reconstructed from a point-by-point measurement, as a function of the pump-probe delay. The spatial extent of the signal, i.e., the width evolution as a function of pump-probe delay time reports on the transport dynamics in the sample (see also Section 3).

Similar to wide-field imaging, existing pump-probe microscopy setups can be upgraded to retrieve spatiotemporal information just by the incorporation of a beam scanner in the probe path. However, careful control of the focusing properties of both the pump and the probe is necessary to ensure good performance, which is experimentally more complex than the widefield alternatives. Nevertheless, point detectors are faster and have a larger dynamic range than cameras. This, together with lock-in demodulation, enables sensitivities that are essentially impossible to reach in a wide-field experiment.

For more detailed information on point-scanning SPTM setups, please see Refs. [2, 12]

2.2.4. Transient Grating Spectroscopy

Transient grating spectroscopy indirectly infers spatial information from a sinusoidal illumination pattern. Conceptually, this approach is similar to point-like pump-excitation. However, rather than using a single point, a spatial high-frequency oscillation imprints spatially localized excitations along one dimension of the image plane. The pump-induced transient complex refractive index change acts as a diffraction grating for the probe beam.[13] As the photoinduced particles or heat diffuse, the initially well-defined grating blurs, leading to a reduced diffraction efficiency of the detected probe. Intrinsic population dynamics contribute to signal decay, but routines that isolate the transport-associated decay exist, as we discuss in more detail below.

The basic layout of a typical transient grating experiment is shown in Figure 2d. It comprises pump and probe pulses, as well as a mechanical delay line alongside a diffraction grating[14] that generates the sinusoidal excitation pattern via pump self-interference. Most systems use the heterodyne detection scheme depicted in Figure 2d[15] where the diffracted probe field, e.g., the signal, interferes with a reference-wave that provides both noiseless signal amplification and background reduction. In this configuration, probe and reference beams are obtained by using the same grating. Pulsed or continuous-wave (CW) probes can be used, depending on the required temporal resolution. If CW lasers are used, the resolution is limited by the temporal response of the detector, typically around 1 ns, but no delay line is required, increasing the maximum observation time and leading to a simpler experimental implementation.

When a diffusing species under investigation has intrinsic decay dynamics, such as electron-hole recombination, it is no longer possible to directly infer transport properties from a single signal decay measurement. However, only the diffusion contribution is proportional to the shape of the excitation profile, e.g., to the period of the sinusoidal exciton pattern. As such, the two signals can be separated, thus isolating the transport information, by performing multiple measurements while systematically varying the grating period,[16] an approach that is also taken in the work summarized in Figure 4b.

Even though transient grating spectroscopy infers the information of interest in an indirect fashion, it is a very mature technique and has proven very flexible regarding the types of samples it can handle. Compared to the methods tracking the evolution of a point-like excitation, transient grating interrogates a larger sample area. As such, it can provide better signal-to-noise ratios at lower photoexcitation densities, a key-advantage for certain applications. However, it necessarily assumes homogeneous and relatively flat samples and only provides limited spatial information on nano- to micro-scales.

For more detailed information on transient grating spectroscopy setups, please see Refs. [15, 17] or this textbook.[13]

3. Transport Theory

In the case of diffusive transport in an isotropic medium, the net velocity of all particles is zero, as it is driven by the random Brownian motion of particles interacting with their environment. In the case of convective transport, the net velocity is nonzero due to a directional field. **Figures 3**a,b illustrates this difference between diffusion and convection. Equation (1) describes convection-diffusion transport:

$$\frac{\partial n_{\mathrm{exc}}}{\partial t} = \underbrace{\nabla \cdot (D \nabla n_{\mathrm{exc}})}_{\text{Diffusion}} - \underbrace{\nabla \cdot (\mathbf{v} \cdot n_{\mathrm{exc}})}_{\text{Convection/drift}} + \underbrace{R}_{\text{Source or sink}} \tag{1}$$

where n_{exc} is an excited density of particles (or their increased temperature), t is time, ∇ is the multi-dimensional gradient, D is

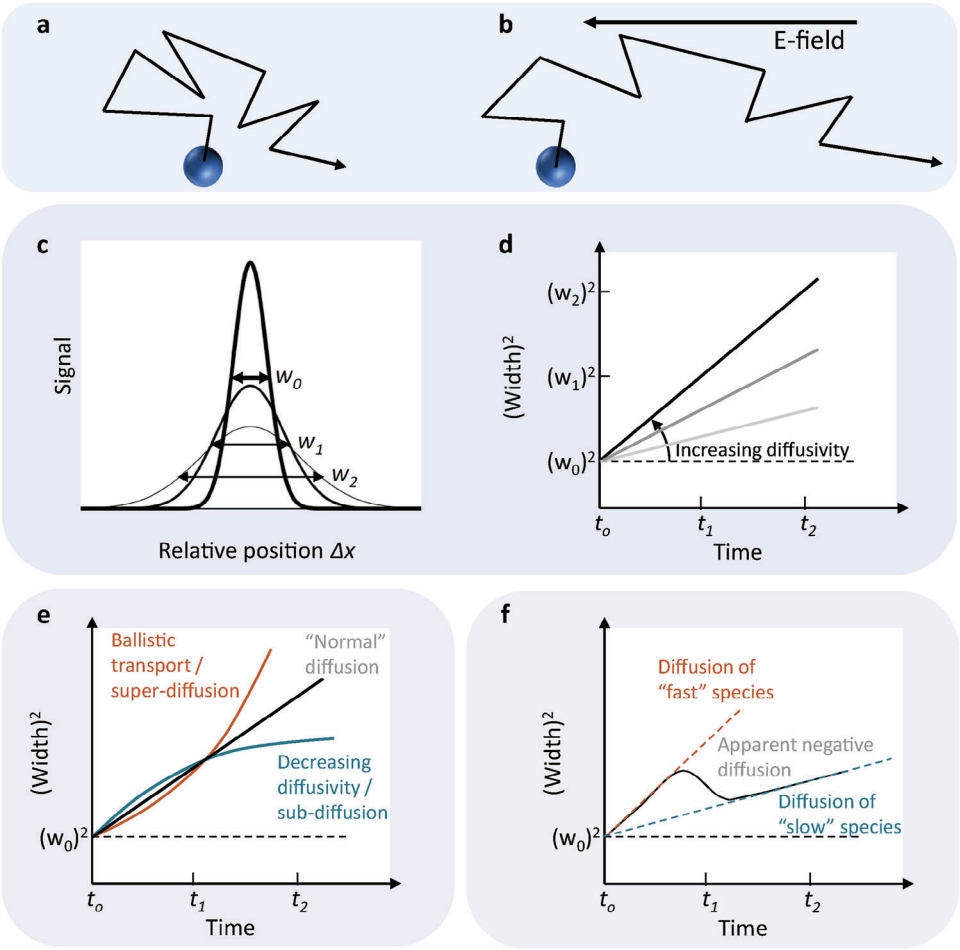

Figure 3. Diffusion, concept and manifestation. a) Schematic representation of diffusive motion of a particle, e.g., an electron, whose mean free path is limited by scattering events. b) Schematic representation of drift-diffusion of an electron, where an electric field is present. c) Typical evolution of spatial profiles as a function of time, showing a decrease of signal and simultaneous spatial broadening. d) In the case of "normal" diffusion, the squared width of the spatial profiles increases linearly with time. A larger slope indicates a larger diffusivity. e) Possible behaviors of the squared width as a function of time for a single diffusing species, with "normal", "super-diffusive", and "sub-diffusive" transport. f) Possible behavior of the squared width as a function of time for two coupled species with different diffusivities – a short-lived fast-diffusing species and a longer-lived slowly-diffusing species. This situation can give rise to apparent negative diffusion.

the diffusivity, **v** is the convection/drift velocity, and R describes any source term or particle/heat sink. In the case of charge transport, "convection" is usually called "drift". Without driving field, the net drift velocity will be zero, and if there is no source or sink present, Equation (1) simplifies to Fick's law of particle diffusion, where **r** indicates position:

$$\frac{\partial n_{\text{exc}}(\mathbf{r},t)}{\partial t} = D_{\text{charge}} \nabla^2 n_{\text{exc}}(\mathbf{r},t) \tag{2}$$

In the case of heat transport without a driving field and no source/sink, Equation (1) simplifies to Fourier's law:

$$\frac{\partial T(\mathbf{r},t)}{\partial t} = D_{\text{heat}} \nabla^2 T(\mathbf{r},t) \tag{3}$$

where $T(\mathbf{r}, t)$ is the time- and position-dependent temperature. This equation is mathematically identical to Fick's law. The diffusivity, D_{charge} or D_{heat}, indicates how efficiently excited charges or heat can spread in space as a function of time (Figure 3c). If particles or heat are created in a Gaussian spot with a certain initial width, then the squared width increases quadratically with time, where the slope is directly proportional to the diffusivity (Figure 3d). For transport in two dimensions, the diffusivity is given by:

$$D = \frac{1}{2}\frac{\partial \sigma^2}{\partial t} = \frac{1}{16\ln(2)}\frac{\partial \text{FWHM}^2}{\partial t} \tag{4}$$

where σ represent the Gaussian width and FWHM is the full width at half maximum.

This is the case for "normal" diffusion. Interestingly, SPTM can also elucidate "nonlinear" diffusion processes. For example, a diffusing species can diffuse increasingly fast (slow), called super-diffusion (sub-diffusion), as depicted in Figure 3e. In the case of two diffusing species that have different diffusivities and that are coupled, the width as a function of time can show a

temporary decrease, corresponding to an apparent negative diffusivity (Figure 3f). The observation of "nonlinear" diffusion can also mean that transport does not take place in the diffusive regime. For example "super-diffusive" behavior can indicate ballistic transport, where transport occurs without scattering. Such observations are made possible by the time-and space-resolved nature of SPTM, and are typically not possible with conventional transport techniques that obtain a time- and space-averaged transport parameter.

In the "normal" diffusive transport regime, the charge diffusivity, with units [ms^{-2}], is directly related to the charge mobility. This is the parameter that determines the drift velocity that occurs upon application of a given electric field, hence its units [ms^{-1}]/[Vm^{-1}] = [$m^2V^{-1}s^{-1}$]. The charge diffusivity and the charge mobility are connected through the following Einstein equations:

$$\underbrace{D_{\text{charge}} = \frac{\mu_{\text{charge}} k_B T}{e}}_{\text{General particles}} \quad \underbrace{D_{\text{charge}} = \frac{\mu_{\text{charge}} E_F}{e}}_{\text{Fermi gas (metal)}} \quad \underbrace{D_{\text{charge}} = \frac{\mu_{\text{charge}} p}{e\frac{\partial p}{\partial \phi}}}_{\text{Semiconductor}} \quad (5)$$

where k_B is the Boltzmann constant, T is temperature, e is elementary charge, E_F is Fermi energy, p is density of states, and ϕ is chemical potential. In the case of heat transport, it is often useful to connect the thermal diffusivity, D_{heat}, to the thermal conductivity, κ, through the heat capacity at constant volume C_V: $\kappa = C_V \cdot D_{\text{heat}}$.

4. Particle Transport Studied Using SPTM

4.1. "Normal" Diffusion of (Quasi)Particles

Time-correlated microscopy has been widely used to study the diffusion of (quasi)particles.[1] Examples include materials such as quantum dot solids,[4] supramolecular nanofibers,[18] organic semiconductors,[5,8,19] inorganic–organic semiconductors, such as 2D layered perovskites,[7,20,21] and inorganic semiconductors, such as transition metal dichalcogenides.[22–24] Among the pioneering time-correlated microscopy works are those by Akselrod et al. who studied exciton transport in tetracene crystals[5] and quantum dot solids[4] on microsecond to nanosecond timescales. In their tetracene work, the authors used pulsed excitation at 400 nm to generate singlet excitons that very rapidly decayed into two triplets. Although triplet states are spin-forbidden from emitting (dark states), delayed fluorescence (i.e., the annihilation of two triplets to form a singlet, followed by emission) can be used to track these quasiparticles. Using time-correlated microscopy, Akselrod et al. determined the anisotropic exciton diffusivities, along the three crystal axis of the tetracene crystal-lattice, to be $D_a = 1.35 \cdot 10^{-3}$ cm^2s^{-1}, $D_b = 2.28 \cdot 10^{-3}$ cm^2s^{-1} and $D_c = 0.31 \cdot 10^{-3}$ cm^2s^{-1} and, further, observed trap-induced deviations from the linear diffusion regime at very long time-delays.[5]

Recently, Lo Gerfo M and coworkers performed excitation beam-scanning based time-correlated microscopy at very low fluences <13 $nJcm^{-2}$, an important step toward studying materials at "operando" fluences e.g., sunlight-like light levels.[8] The authors were able to reduce their excitation intensity to approximately ten suns while directly visualizing spatiotemporal diffusion dynamics in films of Y6 – an organic solar cell material – with various thicknesses. Operating under these conditions allowed the authors to decouple diffusivity measurements from the often encountered parasitic signals due to exciton–exciton annihilation. Their measured diffusion coefficients of 0.017 ± 0.003 cm^2s^{-1} and $D = 0.012 \pm 0.003$ cm^2s^{-1} for 50 and 300 nm films, respectively, were significantly lower than those obtained via alternative, high-fluence, approaches.

Transient grating based approaches have been extensively used for the measurement of the diffusion properties of charge carriers. Among the successful examples are applications to studying exciton diffusion[16] and, more recently, 2D materials such as WSe_2[25] and $MoSe_2$[26] monolayers. Another example are ambipolar mobilities, e.g., the combined electron and hole mobility, in semiconductors[27–29] including the recent observation of high ambipolar mobility and ultra-high thermal conductivity in cubic boron arsenide[30] by the Chen group, a finding that was in parallel reported by Yue et al., using widefield imaging-based transient reflection SPTM:[31] This is a great example of how compatible information can be obtained using different SPTM techniques. The Chen group used femtosecond-pump generated excitation gratings (**Figure** 4b, left), of varying periodicity, and then measured the grating-induced probe deflection as a function of time delay (Figure 4b, top right). The ambipolar diffusivity-induced grating decay was directly observed on short, sub-nanosecond, time scales, an observation that the authors, further, correlated with a measurement of the slower thermal decay, occurring in the nanosecond range (Figure 4b, bottom right). From the measured diffusivities, mobilities are calculated by using the first Einstein equation in Equation (5). By systematically studying samples with varying levels of impurities the authors identified conditions that, simultaneously, enabled high thermal and ambipolar mobilities of up-to 1600 $cm^2V^{-1}s^{-1}$. Using widefield imaging reflection-based SPTM Yue et al.[31] observed comparable ambipolar mobilities, in the 1550 $cm^2V^{-1}s^{-1}$ range (Figure 4c). Yue et al. performed systematic experiments to uncover the effect of hot carrier injection, employing both a blue, 400 nm, as well as a red, 600 nm, pump pulse in combination with red-shifted probe pulses at 530, 585, and 800 nm with the latter being used to monitor the 600 nm pump-induced spatiotemporal dynamics. The authors not only uncovered clear signatures of hot carriers but, further, observed extremely high ambipolar mobilities, as-high-as 5200 $cm^2V^{-1}s^{-1}$, an observation that they attributed to the local doping levels of cubic boron arsenide samples. Widefield imaging-based SPTM has also been employed to studying exciton and charge transport in a variety of materials such as crystalline and amorphous perovskites, TIPS-pentacence, as well as semiconductors[9,10] or more exotic materials such as hybrid, perovskite-based, exciton-polariton systems.[32]

Cross-polarized transient grating schemes have also been implemented by rotating the polarization of one of the pump beams (Figure 2d) by ninety degrees. The result is a polarization oscillation, rather than an amplitude oscillation, in the sample plane. This grating image is composed of fringes of linear and circular polarization, a means of generating a spatially modulated electron spin orientation in multiple quantum well semiconductors, as proposed by Cameron and

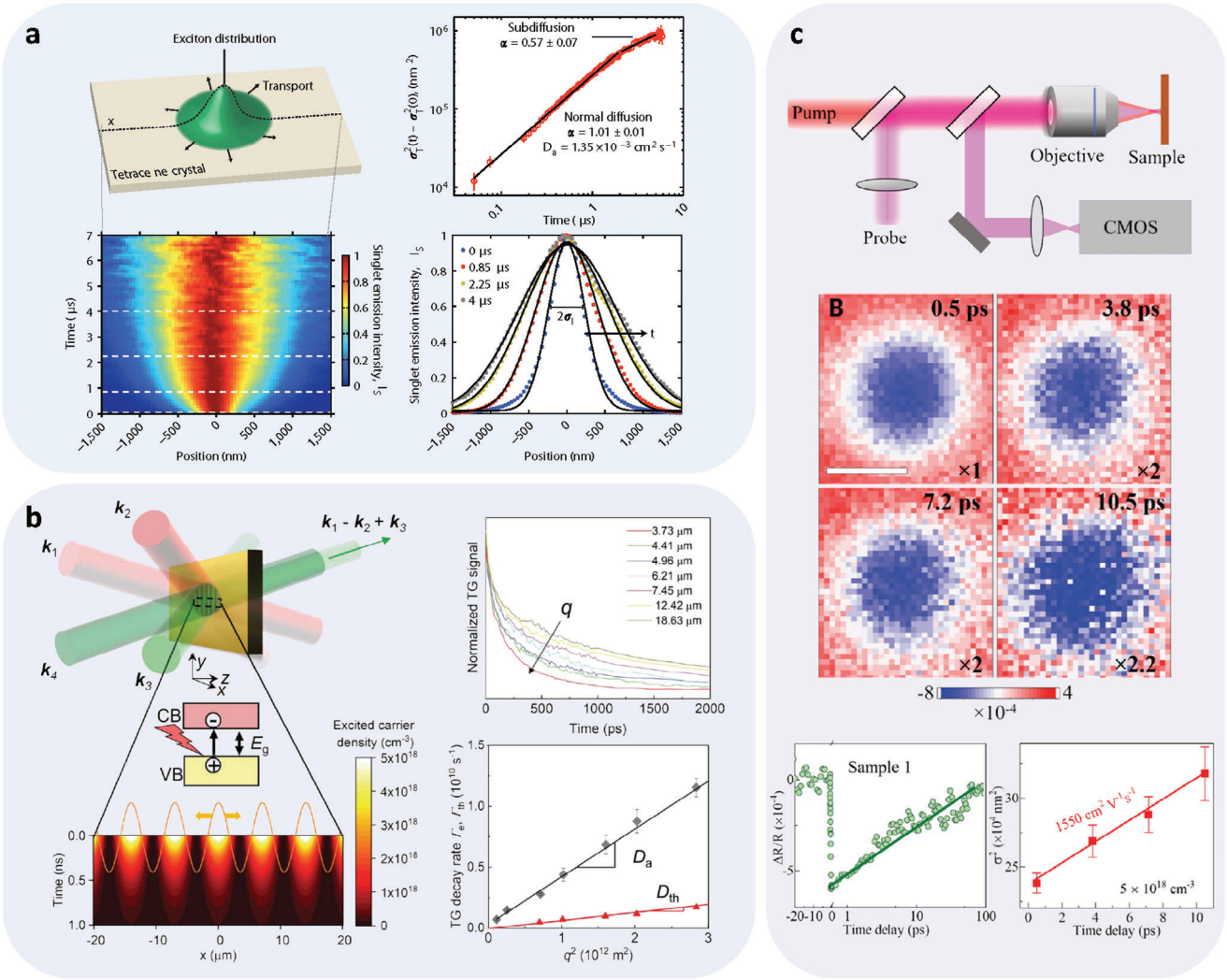

Figure 4. Visualising particle diffusion with SPTM. a) Exciton diffusion in tetracene crystals as studied via time-correlated microscopy. At very long time-delays, deviations from linear diffusion indicate the presence of trap states. Adapted with permission.[5] Copyright 2014, NPG. b) Measuring correlated ambipolar charge and thermal diffusivity with transient grating spectroscopy. Systematically varying the grating period allows extracting both the ambipolar charge diffusivity, D_a, and the thermal diffusivity, D_{th}. Adapted with permission.[30] Copyright 2022, AAAS. c) Visualing ambipolar charge diffusion with widefield SPTM. Adapted with permission.[31] Copyright 2022, AAAS.

co-workers.[33] Following this approach, the authors isolated electron contributions to the ambipolar diffusivity. More recently, the same approach was used to study rapid valley depolarization in 2D materials, occurring within 170 femtoseconds for $MoSe_2$.[26,34]

Point-scanning SPTM has been used to study the (quasi-) particle transport in a host of different materials. Earlier work focused on nanowires, from ensembles of carbon nanotubes,[35] to experiments resolving single nanowires of gold[36] and silicon,[37] to more complex systems and geometries, such as p-i-n junction nanowires,[38] as well as suspended nanowires.[39] Furthermore, the transport of singlet versus triplet excitons, and their interplay, has been studied in tetracene and related molecules[40–42] where Zhu et al. observed orders-of-magnitude slower triplet diffusivities, $D_{triplet}$, around 0.0023–0.006 cm^2s^{-1}, as compared to the singlet exciton diffusivities, $D_{singlet}$, of 2.3-4.5 cm^2s^{-1}.

Exciton diffusion is an active field of research where the group of Hui Zhao made extensive contributions covering bulk semiconductors, such as GaAs,[12] and many 2D materials: graphene,[43] Bi_2Se_3,[44] MoS_2,[45] WSe_2,[46] $MoSe_2$,[47] and ReS_2.[48] The Zhao group also investigated the anisotropic transport properties of black phosphorous where they observed diffusivities of 1300 and 80 cm^2s^{-1} along the respective armchair and zigzag directions of the material.[49] Beyond single 2D materials, they also studied van der Waals heterostructures, such as a vertical stack of $MoSe_2$ and WS_2 (**Figure 5a**).[50] Here, the diffusing species is the charge transfer exciton, which shows a distinct photoluminescence signature centered around 810 nm. Ceballos et al. studied the transport properties of this exciton via point-scanning transient reflection-based spatiotemoral microscopy using a 730 nm pump followed by resonant read-out at 810 nm. They observed a diffusivity of 14 cm^2s^{-1}, a value similar to

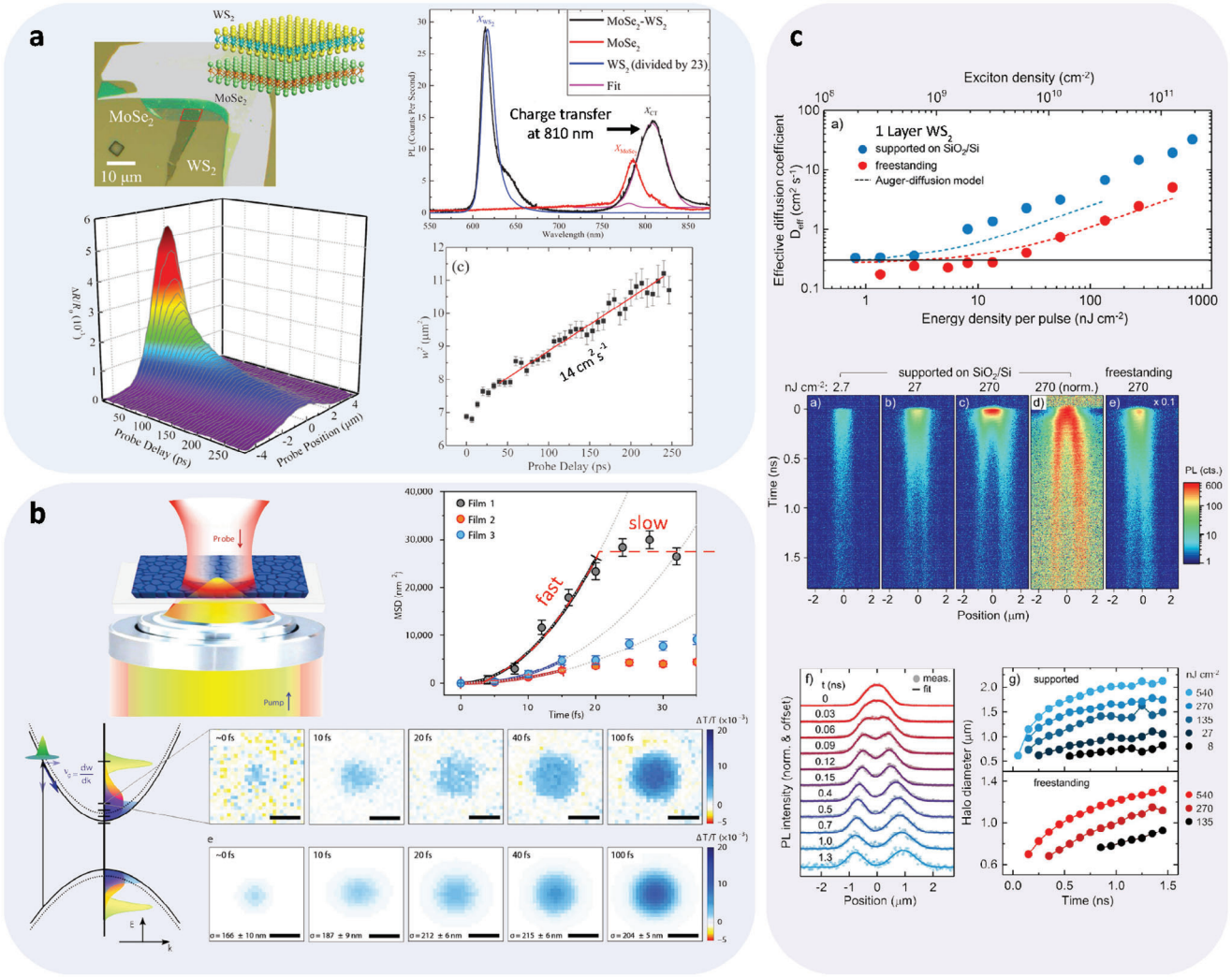

Figure 5. Particle diffusion, from linear to nonlinear diffusivity. a) Point-scanning SPTM yields a diffusivity of 14 cm^2s^{-1} in $MoSe_2$-WS_2. Adapted with permission.[50] Copyright 2015, RSC. b) Sung et al. observed ballistic transport in methylammonium lead iodide pervoskites. Adapted with permission.[52] Copyright 2020, NPG. c) Kulig and coworkers observed exciton halos in monolayer semiconductors. Adapted with permission.[22] Copyright 2018, APS.

the diffusivities of the individual material-monolayers of $MoSe_2$ and WS_2 and concluded that charge-transfer character does not significantly impact the transport behavior. Several other groups also studied exciton diffusion in 2D materials, including studies of drift-diffusion of interlayer excitons.[51]

Finally, the promising class of perovskite materials for photovolatics has also been investigated by point-scanning SPTM.[53–56] Especially the observation of micron-scale structure-diffusion relationships, in the vicinity of grain boundaries, is a great example for the extra information that is provided by SPTM.[56,57]

4.2. Nonlinear Diffusion of (Quasi)Particles

Even samples showing linear diffusivities might transition to sub-diffusive transport when tracked to the very end-tail of the decay where long-lived species can be observed.[5] As pointed out in Section 3, uncovering deviations from the "normal" diffusion regime with sub- or super-diffusive transport behavior (Figure 3e) are an exciting application of SPTM that provides interesting insight into fundamental physics and allows determining ideal operation conditions if linearity is important. Fundamentally, ballistic transport has recently been visualized in lead iodide perovskite thin films by means of ultrafast transient absorption microscopy operating at a very high temporal resolution of 10 fs.[52] The latter was enabled by combining through-objective photoexcitation with a free-space, transmission, probe (Figure 5b) relying on a widefield imaging scheme to detect the spatiotemporal evolution. The authors observed rapid carrier-propagation, covering 50–150 nm during the first 20 fs, followed by a marked change in diffusivity toward scattering-mediated Brownian motion (Figure 5b, bottom). By performing systematic experiments, at varying pump fluences on multiple samples, Sung et al. were able to explain the marked sample-to-sample diffusivity-variations (Figure 5b, top right) by invoking carrier-density dependent scattering probabilities and hence transport

lengths. The authors suggest that charge extraction in perovskite-based light harvesting devices might predominantly occur ballistically, only tens of femtoseconds after carrier injection, a finding that might have important implications for optimizing light harvesting device architectures in general.

Akselrod and coworkers, for the first time, observed the transition from linear to sub-diffusive behavior for exciton transport time delays of >2μs after photoexcitation.[5] They attributed their observation to low-energy trap sites. In 2020 Folie et al.[58] and Seitz et al.[7] independently introduced models to describe the decrease of diffusivity due to permanently trapped excitons, and, shortly after, improvements to account for thermally activated trapping and detrapping were proposed.[10] Thanks to the long temporal regime accessible by time-correlated microscopy, Seitz et al.[21] were able to follow not only the transition from diffusive-to-subdiffusive behavior in 2D-perovskites, via the spatiotemporally resolved emission profile, but also revealed subsequent stagnation and contraction of the latter. They consequently improved the model once more, going beyond a single-trap model and accounting for a distribution of trapping sites.

Importantly, since sub-diffusive behaviors are directly related to trap-quantity and distributions, as well as to the material geometry, time-correlated microscopy allows linking the morphology of the sample to its diffusivity, making it a powerful technique for optimizing the functionality and design of optoelectronic devices.

In the high excitation density regime, more exotic transport behaviors can be observed. Using time-correlated photoluminescence microscopy, Kulig and co-workers[22] observed, for the first time, the formation of ring-shaped spatial emission profiles in monolayer WS_2. These exciton halos, as the authors named the phenomenon, develop only at long time delays and at exciton densities $>10^{10}cm^{-2}$. The authors conducted a pump fluence dependence study, where they observed an apparent diffusivity that, at short times, increases with the laser pulse energy, as shown in Figure 5c (top). This is consistent with a strong Auger recombination contribution, as the initially Gaussian profile evolves in a nonlinear fashion, where the central part decays faster than the tails. This leads to an apparent broadening of the emission and, as a consequence, to an overestimation of the diffusivity. At longer times, the emission profiles continue to evolve. As the central part further reduces, a ring, or halo, emerges (Figure 5c , center and bottom left). As this effect cannot be explained by Auger recombination alone, the authors suggested that an additional memory effect is present. A theoretical follow-up work, by Perea-Causin and co-workers, provided a detailed explanation of the phenomenon,[23] where reabsorption of hot phonons, generated via Auger scattering, generates a strong excitonic temperature gradient. This, in turn, leads to a thermal drift contribution to the transport, that pushes the excitons out of the hot region, thus generating the halo.

5. Heat Transport Studied Using SPTM

5.1. "Normal" Diffusion of Phonon and Electron Heat

Using spatiotemporal wide-field imaging, Delor, and co-workers[10] measured the phonon heat diffusivity of silicon, finding a diffusivity $D_{heat,\,ph}$ of 0.6±0.2 cm^2s^{-1} (**Figure 6a**). This corresponds to a thermal conductivity around 100 $Wm^{-1}K^{-1}$, which is close to the typical thermal conductivity of silicon at room temperature. Interestingly, they could simultaneously resolve charge diffusion with a much larger diffusivity D_{charge} of 35±8 cm^2s^{-1}. These diffusing species – charge versus heat – give rise to a different sign of the transient signal, which makes it easy to distinguish them (Figure 6a). With the same technique, the thermal diffusivity of hBN-encapsulated MoS_2[59] and disordered films of gold nanocrystals[60] were measured recently.

Using point-scanning spatiotemporal reflection microscopy, Block, and co-workers studied the diffusion of both electronic and phononic heat in gold.[61] They observed an initial fast diffusion due to thermalized free charges ($D_{heat,\,el} \approx 95$ cm^2s^{-1}), followed by slower diffusion due to thermalized electrons and phonons, dominated by the phonon diffusivity ($D_{heat,\,ph} \approx 1.1$ cm^2s^{-1}). In a combined experimental-theoretical work, Block et al. observed an intermediate stage of apparent negative diffusion (Figure 6b). The crossover from fast to slow diffusion occurs after a few picoseconds, in agreement with typical interaction timescales, after a short period of apparent negative diffusion.[62]

The group of Hui Zhao used point-scanning microscopy to study the diffusion of electronic heat (hot carriers) in graphene, finding diffusivities between 5,500 and 11,000 cm^2s^{-1}.[43,64] Such large diffusivities are expected given the large charge mobility of graphene (>10,000 $cm^2V^{-1}s^{-1}$), and the direct connection between charge mobility and diffusivity (see Section 3). The authors also observed a transition from initial fast diffusion to slower diffusion after ≈1 ps.[64] This could be related to a similar effect as in gold: the transition from fast electronic heat diffusion to slower phononic heat diffusion.

Recently, Varghese et al. developed a novel type of point-scanning spatiotemporal reflection microscopy technique that gives access to the phonon heat diffusion of suspended films. Their technique exploits the "pre-time-zero" signal, which corresponds to an effective delay of ≈13 ns – the inverse of the repetition rate of their laser (Figure 6c). They used thin suspended flakes, such that no heat dissipation into a substrate could occur, and heat would persist for more than 13 ns, which is observed at a negative time delay. They studied four different transition metal dichalcogenides – $MoSe_2$, WSe_2, MoS_2, and WS_2 – and found phonon heat diffusivities D_{heat} of 0.18 , 0.20 , 0.35 , and 0.59 cm^2s^{-1}, respectively.

Transient grating measurements have been used to study heat diffusion in material systems with broadly varying thermal diffusivities. In a study published in 1995, Käding and co-workers extracted diffusivities ranging from around 0.015 cm^2s^{-1} for fused silica to above 20 cm^2s^{-1} for diamond.[65] Their study also included the bulk materials Ti, Ge, Ni, Mo, Si, Au, Al, SiC, and Cu, where all experimentally determined diffusivities were in agreement with results obtained with alternative techniques, such as time-domain thermoreflectance. They also observed anisotropic diffusion in $BiVO_4$. Figure 6d shows an example of a transient grating experiment, where the thermal conductivity of thin films of PbTe was measured using different grating periods. The authors found a diffusivity $D_{heat,\,ph}$ around 0.013 cm^2s^{-1}.[17] This value is slightly lower than the expected bulk value, which is consistent with thin films typically having a somewhat reduced thermal conductivity. Apart from solid-state materials, also materials

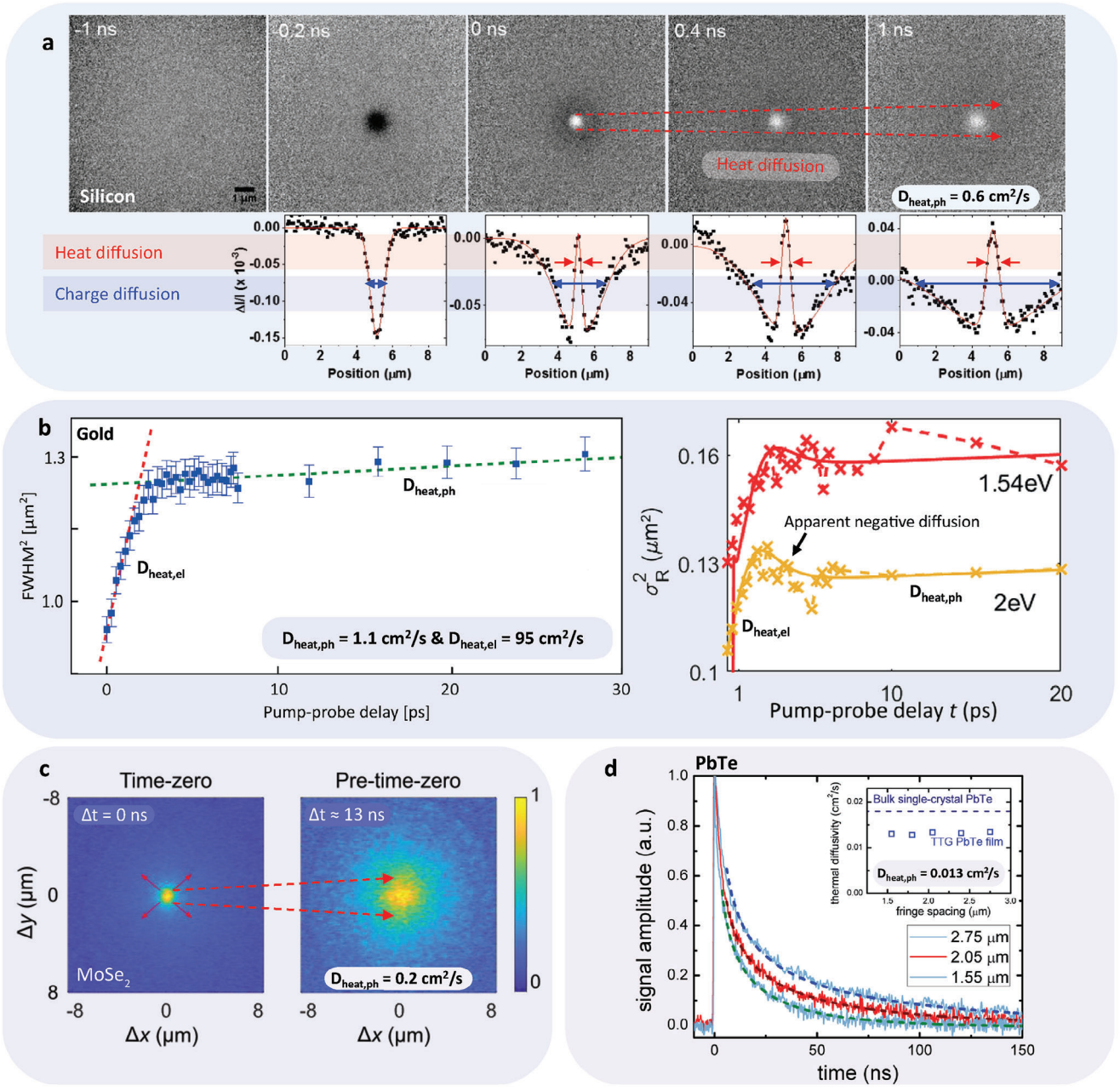

Figure 6. Visualizing heat transport with SPTM. a) Widefield imaging of simultaneous charge diffusion (negative dip in linecuts) and heat diffusion (positive peak in linecuts) in silicon, using the so-called stroboSCAT technique. Adapted with permission.[10] Copyright 2020, NPG. b) Raster-scanned pump-probe reflection measurements of thin gold films, showing fast electronic heat diffusion, followed by slower phononic heat diffusion (left image, adapted with permission.[61] Copyright 2019, AAAS). Apparent negative diffusion is observed around a few picoseconds (right image, adapted with permission.[62] Copyright 2023, ACS). c) Pre-time-zero pump-probe SPTM allows for observing diffusion with an effective delay time of ≈13 ns (inverse of laser repetition rate), in this case yielding the thermal diffusivity of suspended $MoSe_2$. Adapted with permission.[63] Copyright 2023, AIP. d) Signal decay of transient grating measurements on PbTe for different grating periods. From the decay dynamics, the thermal diffusivity is extracted, see inset. Adapted with permission.[17] Copyright 2012, AIP.

in other phases have been studied, such as ionic liquids with thermal diffusivities around and below 0.001 cm^2s^{-1}.[66]

The effect of electron-phonon interactions has also been investigated with transient grating spectroscopy. Using a CW probed setup, Zhou et al.[67] observed a decrease in thermal conductivity of a crystalline silicon membrane when free electrons were induced into the sample tens of nanoseconds after excitation. The authors attributed the effect to an increased phonon scattering by the free carriers, demonstrating the important role of electron–phonon interactions in heat transport.

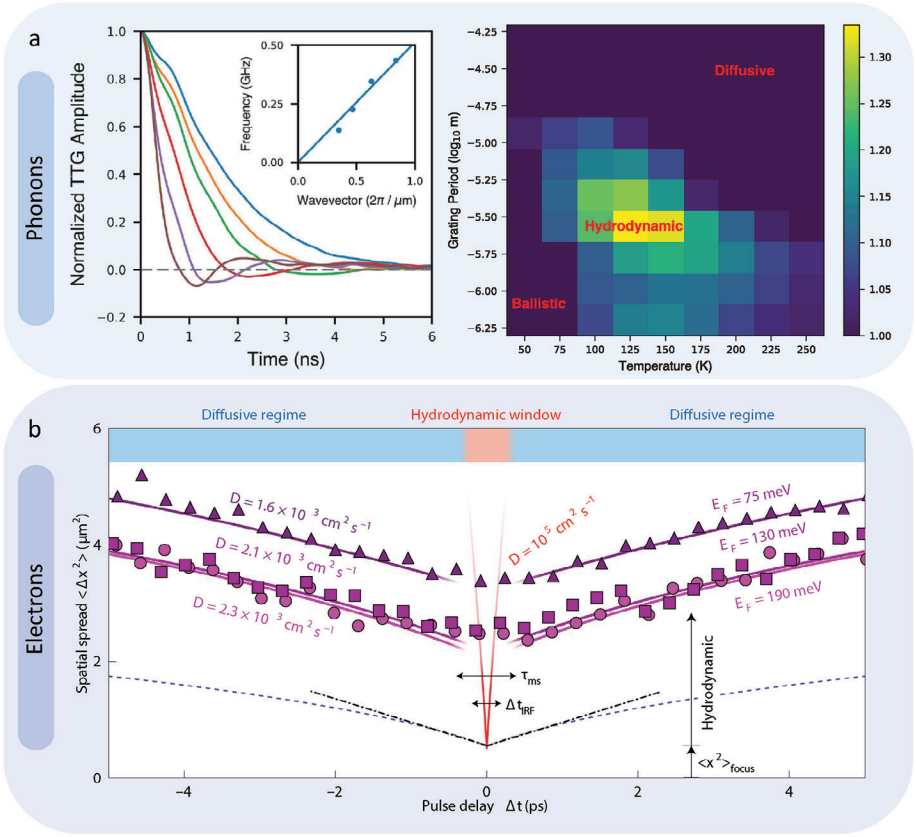

Figure 7. Non-diffusive heat transport. a) Transient grating decay dynamics, showing an unusual sign change after a few nanoseconds, which is a signature of hydrodynamic heat flow. Adapted with permission.[70] Copyright 2019, AAAS. b) Spatiotemporal photocurrent microscopy measurements of electronic diffusion in graphene, showing a crossover from hydrodynamic to diffusive transport of electrons. In the hydrodynamic regime, which lasts a few 100 fs, the electron diffusivity can be two orders of magnitude larger than in the diffusive regime, reaching up to 100,000 cm^2s^{-1}. Adapted with permission.[72] Copyright 2021, NPG.

5.2. Nonlinear Diffusion of Phonon and Electron Heat

In recent years, SPTM techniques have provided access to non-diffusive transport, such as the ballistic and hydrodynamic regime, where heat does not follow conventional laws, such as Fourier's law for phononic heat, or the Wiedemann-Franz law for electronic heat. Transient grating spectroscopy is particularly useful to identify such non-diffusive phenomena, as the sensing length (grating period) can be tuned to be comparable to, or smaller than, the phonons' mean free path, where ballistic heat transport is expected. Johnson and co-workers observed this behavior in freestanding silicon at room temperature,[68] where a deviation from "normal" diffusion was observed by changing the grating period from 10 to 2.4 μm. This was attributed to a significant contribution to the overall heat transport from the low frequency phonons, which show an effective modulation transfer function up to 300 nm. With a similar approach, Robbins and co-workers observed that thermal phonons were able to propagate ballistically across nanocrystalline domains in oriented polymers.[69]

During the past few years, the Nelson and Chen groups detected so-called second sound in graphite, a signature manifestation of hydrodynamic, wave-like, propagation of heat that cannot be explained by the Fourier diffusion model. This was first observed at temperatures up to 100 K using a CW-based transient grating setup with a temporal resolution of 500 ps.[70] Later, it was observed up to 200 K, using a pulsed-probe version of the experiment with picosecond time resolution.[71] In this case, a signature of wave-like heat transport can be observed rather directly: the heterodyned transient grating signal shows damped oscillations with a sign change around 1 ns (**Figure** 7a, left). This sign change indicates that the temperature grating is out of phase with respect to the excitation grating, and indicates a counter-intuitive heat flow from cold to hot spots. This is incompatible with either diffusive or ballistic transport, where heat always flows from hot to cold areas, leading to a gradual washing out of the temperature grating, while staying in phase with the pump. As the heat wave needs to travel half an excitation period to reach the minimum of the signal, the authors used this information to calculate the second sound speed at 3200 ms^{-1}, in good agreement with first principle theoretical calculations (3600 ms^{-1}). The right panel of Figure 7a shows that the hydrodynamic behavior is only present in a particular range of grating periods and temperatures, and not easily observable at room temperature, as this would require very small grating periods.

A crossover from diffusive to hydrodynamic transport-regimes also occurs for the electron system of graphene. In this case, the hydrodynamic regime corresponds to the situation where

electron–electron scattering dominates over other scattering mechanisms, and the system can be interrogated before momentum scattering occurs. Since electron–electron interactions occur on sub-100 fs timescales,[73] one can enter this hydrodynamic regime using high-mobility graphene samples with momentum relaxation times up to several picoseconds. Indeed, a breakdown of the Wiedemann-Franz law, which relates electronic charge transport to electronic heat transport, was observed in the hydrodynamic regime.[74] This observation was made possible by using graphene devices with small dimensions (a few micrometers) and cryogenic temperatures, such that no momentum scattering occurs. However, rather than using small spatial dimensions, one can enter the hydrodynamic heat transport regime by using the time dimension, namely by examining the system at a delay time that is shorter that the momentum relaxation time, a strategy that was recently experimentally realized based on a newly developed spatiotemporal scanning current microscope.[72] Figure 7b shows the main result of these experiments on electrostatically gated graphene. In the diffusive regime, which corresponds to absolute time delays $|\Delta T| > 300$ fs (the momentum relaxation time), the observed broadening is consistent with the expected diffusivity, around 2000 cm^2s^{-1}, based on the – independently measured – charge mobility and the Wiedemann-Franz law, which is equivalent to the Einstein equation in Section 3. These measurements also indicated a strong initial broadening that occurs within the first few hundreds of femtoseconds, corresponding to the hydrodynamic regime. This broadening indicates strongly enhanced thermal transport with an electron heat diffusivity that is two orders of magnitude larger than that in the diffusive regime – up to 100,000 cm^2s^{-1}. Such a strongly increased thermal diffusivity, and strong violation of the Wiedemann-Franz law, is a hallmark of a Dirac fluid, which occurs in the hydrodynamic regime close to the Dirac point.

6. Outlook

During its relatively brief history, SPTM has already had a major impact. It directly visualizes nanoscale mobility and allows one to observe exciting transport phenomena that had previously been difficult or impossible to access. The work summarized in this review is an overview of some of the achievements that have been made over the past years: a solid foundation for many exciting contributions to come. We would like to conclude this review by discussing some potential avenues for future exploration that may expand the scope and applications of SPTM even further.

An exciting new direction is the move toward alternatives to purely optical probing. Time-resolved electron microscopy, in principle, allows observing atomistic motion on ultrafast timescales, an exciting avenue where first steps are being taken.[75,76] Photocurrent readout[72] probes optically difficult to access regions or species and, further, directly reports on device performance. With the emergence of operando imaging and spectroscopy, we believe that photocurrent-based SPTM will play a crucial role for connecting transport dynamics with device functionality and performance.

An important aspect remains interrogating samples under realistic operation conditions, a delicate task given the intrinsically high fluences of pulsed light sources, as compared to sunlight. Promising concepts have been demonstrated, using both linear[8] and nonlinear approaches,[77] but further innovations are needed. Quantum imaging[78,79] or improvements in detection methodologies based on, for example, superconducting nanowires[80,81] are exciting avenues for meeting this challenge.

Further increasing the spectral observation window, both optically and vibrationally, is another area for improvement where only initial steps have been made.[11] Implementing broadband or even multidimensional SPTM would allow separating transport contributions of different species in the often congested spectroscopic observations. Besides photothermal readout, spatially encoded transient spectroscopic information via luminescence,[82,83] infrared spectroscopy,[84] fluorescence encoded infrared spectroscopy,[85] and photoelectron emission,[86] promise to dramatically broaden the applications of SPTM in the future.

As centre-stage in all microscopies, improving the spatial resolution is desirable. Even though SPTM resolves sub-diffraction limited spatial broadening, the technique itself remains diffraction-limited and resolving nanometric structure-function relationships, for example, near interfaces, mismatched crystal-lattices, or grain boundaries is an exciting future direction that calls for creative solutions. Extreme UV excitation,[87,88] holographic,[10,89] tomographic,[90] or quantum imaging[91] all promise to contribute to this outstanding challenge. Other approaches could involve super-resolution techniques, near-field microscopies, and deep-learning frameworks. Finally, an exciting avenue that is emerging is to replace optical beams by electron beams, using transmission and scanning electron microscopy.[92] Owing to the nanometer-scale de Broglie wavelengths of electrons, electron microscopies have the potential to achieve a very high spatial resolution. Indeed, some spatiotemporal studies using electron beams, combined with optical excitation, have recently emerged, such as Refs. [75, 76, 93]. However, for now, we are yet to witness the first truly atomistic movie of heat or carrier transport on ultrafast time scales.

Acknowledgements

G.D.B.V. and G.L.G.M. contributed equally to this work. GDBV, GLGM, and NFvH acknowledged support received through the MCIN/AEI project PRE2019-091051, the "Severo Ochoa" program for Centers of Excellence in R&D CEX2019-000910-S, Fundació Privada Cellex, Fundació Privada Mir-Puig, and the Generalitat de Catalunya through the CERCA program. NFvH acknowledged the financial support by the European Commission (ERC Advanced Grant 101054846-FastTrack). ML was financially supported by the European Union (ERC, PIRO, grant number: 101076859). ICN2 was supported by the Severo Ochoa program from Spanish MINECO Grant No. SEV-2017-0706. KJT. acknowledged funding from the European Union's Horizon 2020 research and innovation program under Grant Agreement No. 804349 (ERC StG CUHL), RYC fellowship No. RYC-2017-22330 and IAE project PID2019-111673GB-I00. Views and opinions expressed are however those of the author(s) only and do not necessarily reflect those of the European Union or the European Research Council. Neither the European Union nor the granting authority can be held responsible for them.

Conflict of Interest

The authors declare no conflict of interest.

Data Availability Statement

The data that are presented in this review are available from the original cited source.

Keywords

charge transport, heat transport, microscopy, spatiotemporal, spectroscopy, ultrafast

Received: August 30, 2023
Revised: October 16, 2023
Published online: November 23, 2023

[1] N. S. Ginsberg, W. A. Tisdale, *Annu. Rev. Phys. Chem.* **2020**, *71*, 1.
[2] T. Zhu, J. M. Snaider, L. Yuan, L. Huang, *Annu. Rev. Phys. Chem.* **2019**, *70*, 219.
[3] A. M. Müller, C. J. Bardeen, *J. Phys. Chem. C* **2007**, *111*, 12483.
[4] G. M. Akselrod, F. Prins, L. V. Poulikakos, E. M. Lee, M. C. Weidman, A. J. Mork, A. P. Willard, V. Bulovic, W. A. Tisdale, *Nano Lett.* **2014**, *14*, 3556.
[5] G. M. Akselrod, P. B. Deotare, N. J. Thompson, J. Lee, W. A. Tisdale, M. A. Baldo, V. M. Menon, V. Bulović, *Nat. Commun.* **2014**, *5*, 3646.
[6] A. M. Berghuis, T. Raziman, A. Halpin, S. Wang, A. G. Curto, J. G. Rivas, *J. Phys. Chem. Lett.* **2021**, *12*, 1360.
[7] M. Seitz, A. J. Magdaleno, N. Alcázar-Cano, M. Meléndez, T. J. Lubbers, S. W. Walraven, S. Pakdel, E. Prada, R. Delgado-Buscalioni, F. Prins, *Nat. Commun.* **2020**, *11*, 2035.
[8] G. Lo Gerfo M, L. Bolzonello, F. Bernal-Texca, J. Martorell, N. F. van Hulst, *J. Phys. Chem. Lett.* **2023**, *14*, 1999.
[9] M. Delor, A. H. Slavney, N. R. Wolf, M. R. Filip, J. B. Neaton, H. I. Karunadasa, N. S. Ginsberg, *ACS Energy Lett.* **2020**, *5*, 1337.
[10] M. Delor, H. L. Weaver, Q. Q. Yu, N. S. Ginsberg, *Nat. Mater.* **2020**, *19*, 56.
[11] C. Schnedermann, J. Sung, R. Pandya, S. D. Verma, R. Y. S. Chen, N. Gauriot, H. M. Bretscher, P. Kukura, A. Rao, *J. Phys. Chem. Lett.* **2019**, *10*, 6727.
[12] B. A. Ruzicka, L. K. Werake, H. Samassekou, H. Zhao, *Appl. Phys. Lett.* **2010**, *97*, 262119.
[13] H. J. Eichler, P. Günter, D. W. Pohl, *Laser-induced dynamic gratings*, vol. *50*, Springer, Berlin **2013**.
[14] A. Maznev, T. Crimmins, K. Nelson, *Opt. Lett.* **1998**, *23*, 1378.
[15] A. A. Maznev, K. A. Nelson, J. A. Rogers, *Opt. Lett.* **1998**, *23*, 1319.
[16] T. S. Rose, R. Righini, M. Fayer, *Chem. Phys. Lett.* **1984**, *106*, 13.
[17] J. A. Johnson, A. A. Maznev, M. T. Bulsara, E. A. Fitzgerald, T. Harman, S. Calawa, C. Vineis, G. Turner, K. A. Nelson, *J. Appl. Phys.* **2012**, *111*, 023503.
[18] B. Wittmann, F. A. Wenzel, S. Wiesneth, A. T. Haedler, M. Drechsler, K. Kreger, J. Köhler, E. W. Meijer, H.-W. Schmidt, R. Hildner, *J. Am. Chem. Soc.* **2020**, *142*, 8323.
[19] B. Wittmann, S. Wiesneth, S. Motamen, L. Simon, F. Serein-Spirau, G. Reiter, R. Hildner, *J. Chem. Phys.* **2020**, *153*, 144202.
[20] X. Xiao, M. Wu, Z. Ni, S. Xu, S. Chen, J. Hu, P. N. Rudd, W. You, J. Huang, *Adv. Mater.* **2020**, *32*, 2004080.
[21] M. Seitz, M. Meléndez, N. Alcázar-Cano, D. N. Congreve, R. Delgado-Buscalioni, F. Prins, *Adv. Opt. Mater.* **2021**, *9*, 2001875.
[22] M. Kulig, J. Zipfel, P. Nagler, S. Blanter, C. Schüller, T. Korn, N. Paradiso, M. M. Glazov, A. Chernikov, *Phys. Rev. Lett.* **2018**, *120*, 207401.
[23] R. Perea-Causin, S. Brem, R. Rosati, R. Jago, M. Kulig, J. D. Ziegler, J. Zipfel, A. Chernikov, E. Malic, *Nano Lett.* **2019**, *19*, 7317.
[24] R. Rosati, R. Perea-Causín, S. Brem, E. Malic, *Nanoscale* **2020**, *12*, 356.
[25] J. Wang, Y. Guo, Y. Huang, H. Luo, X. Zhou, C. Gu, B. Liu, *Appl. Phys. Lett.* **2019**, *115*, 131902.
[26] H. Kuhn, J. Wagner, S. Han, R. Bernhardt, Y. Gao, L. Xiao, J. Zhu, P. H. van Loosdrecht, *Laser Photonics Rev.* **2020**, *14*, 2000029.
[27] K. Jaraŝiūnas, H. Gerritsen, *Appl. Phys. Lett.* **1978**, *33*, 190.
[28] D. Webber, C. Clegg, A. Mason, S. March, I. Hill, K. Hall, *Appl. Phys. Lett.* **2017**, *111*, 121905.
[29] P. Scajev, C. Qin, R. Aleksiejūnas, P. Baronas, S. Miasojedovas, T. Fujihara, T. Matsushima, C. Adachi, S. Juršėnas, *J. Phys. Chem. Lett.* **2018**, *9*, 3167.
[30] J. Shin, G. A. Gamage, Z. Ding, K. Chen, F. Tian, X. Qian, J. Zhou, H. Lee, J. Zhou, L. Shi, T. Nguyen, F. Han, M. Li, D. Broido, A. Schmidt, Z. Ren, G. Chen, *Science* **2022**, *377*, 437.
[31] S. Yue, F. Tian, X. Sui, M. Mohebinia, X. Wu, T. Tong, Z. Wang, B. Wu, Q. Zhang, Z. Ren, J. Bao, X. Liu, *Science* **2022**, *377*, 433.
[32] D. Xu, A. Mandal, J. M. Baxter, S.-W. Cheng, I. Lee, H. Su, S. Liu, D. R. Reichman, M. Delo, *Nat. Commun.* **2023**, *14*, 3881.
[33] A. Cameron, P. Riblet, A. Miller, *Phys. Rev. Lett.* **1996**, *76*, 4793.
[34] J. Wagner, H. Kuhn, R. Bernhardt, J. Zhu, P. H. van Loosdrecht, *2D Mater.* **2021**, *8*, 035018.
[35] B. A. Ruzicka, R. Wang, J. Lohrman, S. Ren, H. Zhao, *Phys. Rev. B* **2012**, *86*, 205417.
[36] S. S. Lo, H. Y. Shi, L. Huang, G. V. Hartland, *Opt. Lett.* **2013**, *38*, 1265.
[37] M. M. Gabriel, J. R. Kirschbrown, J. D. Christesen, C. W. Pinion, D. F. Zigler, E. M. Grumstrup, B. P. Mehl, E. E. Cating, J. F. Cahoon, J. M. Papanikolas, *Nano Lett.* **2013**, *13*, 1336.
[38] M. M. Gabriel, E. M. Grumstrup, J. R. Kirschbrown, C. W. Pinion, J. D. Christesen, D. F. Zigler, E. E. Cating, J. F. Cahoon, J. M. Papanikolas, *Nano Lett.* **2014**, *14*, 3079.
[39] E. E. M. Cating, C. W. Pinion, E. M. Van Goethem, M. M. Gabriel, J. F. Cahoon, J. M. Papanikolas, *Nano Lett.* **2016**, *16*, 434.
[40] Y. Wan, Z. Guo, T. Zhu, S. Yan, J. Johnson, L. Huang, *Nat. Chem.* **2015**, *7*, 785.
[41] T. Zhu, Y. Wan, Z. Guo, J. Johnson, L. Huang, *Adv. Mater.* **2016**, *28*, 7539.
[42] T. Zhu, Y. Wan, L. Huang, *Acc. Chem. Res.* **2017**, *50*, 1725.
[43] B. A. Ruzicka, S. Wang, L. K. Werake, B. Weintrub, K. P. Loh, H. Zhao, *Phys. Rev. B* **2010**, *82*, 195414.
[44] N. Kumar, B. A. Ruzicka, N. P. Butch, P. Syers, K. Kirshenbaum, J. Paglione, H. Zhao, *Phys. Rev. B* **2011**, *83*, 235306.
[45] R. Wang, B. A. Ruzicka, N. Kumar, M. Z. Bellus, H. Y. Chiu, H. Zhao, *Phys. Rev. B* **2012**, *86*, 045406.
[46] Q. Cui, F. Ceballos, N. Kumar, H. Zhao, *ACS Nano* **2014**, *8*, 2970.
[47] N. Kumar, Q. Cui, F. Ceballos, D. He, Y. Wang, H. Zhao, *Nanoscale* **2014**, *6*, 4915.
[48] Q. Cui, J. He, M. Z. Bellus, M. Mirzokarimov, T. Hofmann, H. Y. Chiu, M. Antonik, D. He, Y. Wang, H. Zhao, *Small* **2015**, *11*, 5565.
[49] J. He, D. He, Y. Wang, Q. Cui, M. Z. Bellus, H.-Y. Chiu, H. Zhao, *ACS Nano* **2015**, *9*, 6436.
[50] F. Ceballos, M. Z. Bellus, H.-Y. Chiu, H. Zhao, *Nanoscale* **2015**, *7*, 17523.
[51] Z. Sun, A. Ciarrocchi, F. Tagarelli, J. F. Gonzalez Marin, K. Watanabe, T. Taniguchi, A. Kis, *Nat. Photonics* **2022**, *16*, 79.
[52] J. Sung, C. Schnedermann, L. Ni, A. Sadhanala, R. Y. Chen, C. Cho, L. Priest, J. M. Lim, H.-K. Kim, B. Monserrat, P. Kukura, A. Rao, *Nat. Phys.* **2020**, *16*, 171.
[53] Z. Guo, J. S. Manser, Y. Wan, P. V. Kamat, L. Huang, *Nat. Commun.* **2015**, *6*, 7471.
[54] Z. Guo, Y. Wan, M. Yang, J. Snaider, K. Zhu, L. Huang, *Science* **2017**, *356*, 59.
[55] T. Zhu, Y. Wan, L. Huang, *Acc. Chem. Res.* **2017**, *50*, 1725.
[56] S. Deng, D. D. Blach, L. Jin, L. Huang, *Adv. Energy Mater.* **2020**, *10*, 1903781.

[57] J. M. Snaider, Z. Guo, T. Wang, M. Yang, L. Yuan, K. Zhu, L. Huang, *ACS Energy Lett.* **2018**, *3*, 1402.
[58] B. D. Folie, J. A. Tan, J. Huang, P. C. Sercel, M. Delor, M. Lai, J. L. Lyons, N. Bernstein, A. L. Efros, P. Yang, N. S. Ginsberg, *J. Phys. Chem. A* **2020**, *124*, 1867.
[59] H. L. Weaver, C. M. Went, J. Wong, D. Jasrasaria, E. Rabani, H. A. Atwater, N. S. Ginsberg, arxiv **2023**, 2305.13676.
[60] J. K. Utterback, A. Sood, I. Coropceanu, B. Guzelturk, D. V. Talapin, A. M. Lindenberg, N. S. Ginsberg, *Nano Lett.* **2021**, *21*, 3540.
[61] A. Block, M. Liebel, R. Yu, M. Spector, Y. Sivan, F. J. García de Abajo, N. F. Van Hulst, *Sci. Adv.* **2019**, *5*, eaav8965.
[62] A. Block, R. Yu, I.-W. Un, S. Varghese, M. Liebel, N. F. van Hulst, S. Fan, K.-J. Tielrooij, Y. Sivan, *ACS Photonics* **2023**, *10*, 1150.
[63] S. Varghese, J. D. Mehew, A. Block, D. S. Reig, P. Woźniak, R. Farris, Z. Zanolli, P. Ordejón, M. J. Verstraete, N. F. Van Hulst, K. J. Tielrooij, *Rev. Sci. Instrum* **2023**, *94*, 034903.
[64] B. A. Ruzicka, S. Wang, J. Liu, K.-P. Loh, J. Z. Wu, H. Zhao, *Opt. Mater. Express* **2012**, *2*, 708.
[65] O. Käding, H. Skurk, A. Maznev, E. Matthias, *Appl. Phys. A* **1995**, *61*, 253.
[66] C. Frez, G. J. Diebold, C. D. Tran, S. Yu, *J. Chem. Eng. Data* **2006**, *51*, 1250.
[67] J. Zhou, H. D. Shin, K. Chen, B. Song, R. A. Duncan, Q. Xu, A. A. Maznev, K. A. Nelson, G. Chen, *Nat. Commun.* **2020**, *11*, 6040.
[68] J. A. Johnson, A. Maznev, J. Cuffe, J. K. Eliason, A. J. Minnich, T. Kehoe, C. M. S. Torres, G. Chen, K. A. Nelson, *Phys. Rev. Lett.* **2013**, *110*, 025901.
[69] A. B. Robbins, S. X. Drakopoulos, I. Martin-Fabiani, S. Ronca, A. J. Minnich, *Proc. Natl. Acad. Sci.* **2019**, *116*, 17163.
[70] S. Huberman, R. A. Duncan, K. Chen, B. Song, V. Chiloyan, Z. Ding, A. A. Maznev, G. Chen, K. A. Nelson, *Science* **2019**, *364*, 375.
[71] Z. Ding, K. Chen, B. Song, J. Shin, A. A. Maznev, K. A. Nelson, G. Chen, *Nat. Commun.* **2022**, *13*, 285.
[72] A. Block, A. Principi, N. C. Hesp, A. W. Cummings, M. Liebel, K. Watanabe, T. Taniguchi, S. Roche, F. H. Koppens, N. F. van Hulst, K.-J. Tielrooij, *Nat. Nanotechnol.* **2021**, *16*, 1195.
[73] M. Massicotte, G. Soavi, A. Principi, K.-J. Tielrooij, *Nanoscale* **2021**, *13*, 8376.
[74] J. Crossno, J. K. Shi, K. Wang, X. Liu, A. Harzheim, A. Lucas, S. Sachdev, P. Kim, T. Taniguchi, K. Watanabe, T. A. Ohki, K. C. Fong, *Science* **2016**, *351*, 1058.
[75] Y. Kurman, R. Dahan, H. H. Sheinfux, K. Wang, M. Yannai, Y. Adiv, O. Reinhardt, L. H. G. Tizei, S. Y. Woo, J. Li, J. H. Edgar, M. Kociak, F. H. L. Koppens, I. Kaminer, *Science* **2021**, *372*, 1181.
[76] D. Cremons, D. Plemmons, D. Flannigan, *Nat. Commun.* **2016**, *7*, 11230.
[77] M. Hörmann, F. Visentin, A. Zanetta, J. Osmond, G. Grancini, N. F. Hulst, M. Liebel, G. Cerullo, F. V. A. Camargo, *Ultrafast Sci.* **2023**, *3*, 0032.
[78] S. Mukamel, M. Freyberger, W. Schleich, M. Bellini, A. Zavatta, G. Leuchs, C. Silberhorn, R. W. Boyd, L. L. Sánchez-Soto, A. Stefanov, M. Barbieri, A. Paterova, L. Krivitsky, S. Shwartz, K. Tamasaku, K. Dorfman, F. Schlawin, V. Sandoghdar, M. Raymer, A. Marcus, O. Varnavski, T. Goodson, Z.-Y. Zhou, B.-S. Shi, S. Asban, M. Scully, G. Agarwal, T. Peng, A. V. Sokolov, Z.-D. Zhang, et al., *J. Phys. B: At., Mol. Opt. Phys.* **2020**, *53*, 072002.
[79] M. Gilaberte Basset, F. Setzpfandt, F. Steinlechner, E. Beckert, T. Pertsch, M. Gräfe, *Laser Photonics Rev.* **2019**, *13*, 1900097.
[80] C. M. Natarajan, M. G. Tanner, R. H. Hadfield, *Supercond. Sci. Technol.* **2012**, *25*, 063001.
[81] I. Esmaeil Zadeh, J. Chang, J. W. N. Los, S. Gyger, A. W. Elshaari, S. Steinhauer, S. N. Dorenbos, V. Zwiller, *Appl. Phys. Lett.* **2021**, *118*, 190502.
[82] S. Goetz, D. Li, V. Kolb, J. Pflaum, T. Brixner, *Opt. Express* **2018**, *26*, 3915.
[83] M. Liebel, C. Toninelli, N. F. van Hulst, *Nat. Photon.* **2018**, *12*, 45.
[84] C. R. Baiz, D. Schach, A. Tokmakoff, *Opt. Express* **2014**, *22*, 18724.
[85] L. Whaley-Mayda, A. Guha, A. Tokmakoff, *J. Chem. Phys.* **2022**, *156*, 174202.
[86] M. Aeschlimann, T. Brixner, A. Fischer, C. Kramer, P. Melchior, W. Pfeiffer, C. Schneider, C. Strüber, P. Tuchscherer, D. V. Voronine, *Science* **2011**, *333*, 1723.
[87] F. Bencivenga, R. Mincigrucci, F. Capotondi, L. Foglia, D. Naumenko, A. Maznev, E. Pedersoli, A. Simoncig, F. Caporaletti, V. Chiloyan, R. Cucini, F. Dallari, R. A. Duncan, T. D. Frazer, G. Gaio, A. Gessini, L. Giannessi, S. Huberman, H. Kapteyn, J. Knobloch, G. Kurdi, N. Mahne, M. Manfredda, A. Martinelli, M. Murnane, E. Principi, L. Raimondi, S. Spampinati, C. Spezzani, M. Trovó, et al., *Sci. Adv.* **2019**, *5*, eaaw5805.
[88] L. Foglia, R. Mincigrucci, A. Maznev, G. Baldi, F. Capotondi, F. Caporaletti, R. Comin, D. De Angelis, R. Duncan, D. Fainozzi, G. Kurdi, J. Li, A. Martinelli, C. Masciovecchio, G. Monaco, A. Milloch, K. Nelson, C. Occhialini, M. Pancaldi, E. Pedersoli, A. Pelli-Cresi, J. S. andn Simoncig, B. Travasso, F. Wehinger, M. Zanatta, F. Bencivenga, *Photoacoustics* **2023**, *29*, 100453.
[89] M. Liebel, F. V. A. Camargo, G. Cerullo, N. F. van Hulst, *Nano Lett.* **2021**, *21*, 1666.
[90] S. Shin, J. Eun, S. S. Lee, C. Lee, H. Hugonnet, D. K. Yoon, S.-H. Kim, J. Jeong, Y. Park, *Nat. Mater.* **2022**, *21*, 317.
[91] R. Camphausen, A. S. Perna, Álvaro Cuevas, A. Demuth, J. A. Chillón, M. Gräfe, F. Steinlechner, V. Pruneri, *Opt. Express* **2023**, *31*, 6039.
[92] W. E. King, G. H. Campbell, A. Frank, B. Reed, J. F. Schmerge, B. J. Siwick, B. C. Stuart, P. M. Weber, *J. Appl. Phys.* **2005**, *97*, 11.
[93] T. T. Lummen, R. J. Lamb, G. Berruto, T. Lagrange, L. Dal Negro, F. J. García De Abajo, D. McGrouther, B. Barwick, F. Carbone, *Nat. Commun.* **2016**, *7*, 13156.

Matz Liebel is an Assistant Professor in Physics at the Vrije Universiteit Amsterdam, the Netherlands. As a member of the Biophotonics & Medical Imaging section, he leads an interdisciplinary research group that combines fundamental with applied research (www.matzlab.com). Matz obtained his DPhil from the University of Oxford, United Kingdom, in 2014. His research, supported by an ERC Starting Grant and an EIC Pathfinder grant, focuses on methodology development in the context of nanosizing, phototransient, and label-free imaging for applications in biology, biomedicine, diagnostics, and the pharmaceutical industry.

Klaas-Jan Tielrooij is an Associate Professor at Eindhoven University of Technology in Eindhoven, the Netherlands, and Senior Group Leader at the Catalan Institute of Nanoscience and Nanotechnology (ICN2) in Barcelona, Spain. He leads a research group called Ultrafast Dynamics in Nanoscale Systems (www.ultrafastdynamics.com). He obtained his PhD from the University of Amsterdam in 2011, the Netherlands, and was awarded the national Physics Thesis Prize 2011. Among his obtained funding are an ERC Starting Grant and ERC Proof of Concept grant. His main interests are in the field of ultrafast dynamics, optoelectronics, nonlinear optics, terahertz technologies, light-matter interaction, and quantum materials.